▼ Journal of Research (Science)
ISSN (print) 1021-1012. ISSN (Online) 3007-1968
Vol. 34, No. 2 July, 2024, pp. 100-113
DOI: https://doi.org/10.64762/2e6gjy40
https://jorscience.com/

FABRICATION OF G-C_3N_4/NIO/ZNO BASED TERNARY NANOCOMPOSITE FOR EFFICIENT PHOTOCATALYTIC DEGRADATION OF METHYLENE BLUE

Nimra Zafar[1], Affaf Sajjad[2], Rida Fatima[2], Taimoor Abbas[3], Muhammad Ajmal Khan[4], Muhammad Meesum Bilal[5], Uzma Bilal[2], Hafiz Muhammad Noman[2], Abu Summama Sadavi Bilal[2*]

[1]Polymer and Textile Engineering, University of Punjab, Lahore, Pakistan
[2]Faculty of Sustainable Design Engineering (FSDE), University of Prince Edward Island, Charlottetown, PE 5C1A 4P3, Canada
[3]Institute of Environmental Science and Engineering (IESE), National University of Science and Technology (NUST), H-12 Campus, Islamabad 44000, Pakistan
[4]Department of Physics, Clean Energy Research Lab (CERL), COMSATS University Islamabad, Lahore Campus, Lahore, Pakistan
[5]Hefei National Laboratory for Physical Science at Microscale, School of Physical Sciences, Department of Modern Physics. University of Science and technology of China, Hefei 230026, Anhui, P.R. China
***Corresponding authors:** abilal@upei.ca*

Abstract

Photocatalysis has emerged as a widely recognized and environmentally friendly technique for the degradation of biological contaminants into less hazardous substances. The technique offers a sustainable path for contamination reduction by utilizing sunlight-activated catalysts to initiate reactions for the degradation of pollutants. In this work, a facile co-precipitation approach was utilized to synthesize a ternary nanocomposite-based photocatalyst to improve photocatalytic performance. The metal oxide semiconductors ZnO and NiO were successfully integrated into the g-C_3N_4 matrix to develop a photocatalyst that showed substantially increased photocatalytic activity. The synthesized ternary nanocomposite was investigated for different physicochemical techniques such as photoluminescence (PL), ultraviolet-visible (UV-Vis) absorption spectroscopy, scanning electron microscopy (SEM), Raman spectroscopy, and X-ray diffraction (XRD). The structural, morphological, and optical characteristics of the ternary nanocomposite were thoroughly explored by these physiochemical techniques. The synthesized CNZ ternary nanocomposites-based photocatalyst revealed a significantly enhanced photocatalytic degradation rate of 92%, outperforming all other samples. The ternary nanocomposite demonstrated excellent reusability even after five successive reaction cycles, unveiling the superior potential in the photocatalytic application for an extended period without significantly losing its effectiveness. The synergistic integration of NiO and ZnO into g-C_3N_4 boosted the photocatalytic activity by enhancing electron-hole separation and reducing recombination reactions. The hybrid photocatalyst offers a great deal of promise for effectively eliminating harmful pollutants from aqueous solutions.

Keywords: g-C_3N_4/NiO/ZnO, ternary nanocomposite, methylene blue, photocatalysis.

INTRODUCTION

In order to solve the persuasive concerns of expanding global energy demand and escalating environmental challenges, it is now imperative to explore and utilize renewable

Article type: Research Paper; **Section:** Engineering & Technological Innovations; **Section Editor:** Dr Engr Akbar Ali Qureshi
History: Received: 24 Jun, 2025; **Accepted:** 30 Jun, 2025; **In Press**: 28 Jul, 2025; **Published**: 9 Aug, 2025

and clean energy sources (Algarni et al., 2023; Sikiru et al., 2024; L. Zhang et al., 2024). Wastewater discharged from various industrial and medical activities that contains significant amounts of dyes and medicines poses a significant threat to ecological health and is a major obstacle to environmental hygiene (Alsukaibi, 2022; Onu et al., 2023; Samrot et al., 2023). For the treatment of water polluted with organic contaminants, advanced oxidation processes (AOPs) such as photocatalytic oxidation mechanisms are well-established techniques (Khader et al., 2024). These techniques are essential for applications involving water purification since they are remarkably effective at breaking down complex organic molecules (Nishu & Kumar, 2023). Photocatalysis is now considered to be a very flexible and promising approach with a wide range of applications including wastewater purification, microbial disinfection, and the decomposition of hazardous organic compounds (Xu et al., 2022; J. Zhang et al., 2024). As the method utilizes photocatalysts to initiate catalytic activities, this approach to treating many environmental challenges is sustainable and beneficial for the environment. The immense potential of semiconductor-based photocatalysis in energy and environmental applications, including water splitting for the generation of hydrogen and oxygen, oxidation of organic pollutants, and reduction of carbon dioxide, has triggered a lot of attraction (Chen et al., 2021; Yang et al., 2022). This approach produces electron-hole pairs that may efficiently initiate and drive these chemical processes by absorbing photons with energies higher than the semiconductor bandgap (Zhang et al., 2023). The majority of semiconductor photocatalysts, including the extensively investigated ZnO, WO_3, SnO_2, TiO_2, CeO_2, ZnS, and ZrO_2, normally have a single metal center (Bhapkar & Bhame, 2024; Sahu & Chopra, 2023; Zeinali Heris et al., 2023).

Among others, Wurtzite ZnO (*n*-type semiconductor) is renowned for its exceptional characteristics, which include low production costs, unique electrical structure, outstanding chemical stability, and biocompatibility (Kahouli et al., 2015; Raha & Ahmaruzzaman, 2022). It is widely used in several photocatalytic energy conversion applications. ZnO has a large exciton binding energy and a UV-active band gap of 3.37 eV at ambient temperature. Its broad and useful application in photocatalysis is nevertheless constrained by its large band gap and excessive recombination rate (Beura et al., 2018; Han et al., 2012). This limitation is addressed by sensitizing ZnO with narrow band gap semiconductors, such as g-C_3N_4, which causes its absorption band to shift into the visible spectrum. ZnO/polymer and ZnO/metal oxide hybrid nanocomposites have demonstrated visible-light photodegradation activity. This occurs due to the formation of intermediate states in photocatalysts, subsequently promoting the absorption of visible light and encouraging the generation of electron holes during the photoreaction process (Kumaresan et al., 2020; Qiu et al., 2008; Toma et al., 2022).

Nickel oxide (NiO) is another semiconductor (*p*-type) renowned for its remarkable hole mobility and high theoretical specific capacitance making it a highly desirable contender for applications in a variety of sectors such as dye-sensitized solar cells and supercapacitors (Flores-Diaz et al., 2023; Natu et al., 2012). Furthermore, NiO may be used to build p-n heterojunctions with a variety of n-type materials primarily due to its wide bandgap (Wang et al., 2022). By reducing the recombination of photogenerated electron-hole pairs, these heterojunctions efficiently increase the efficiency of photocatalysis. The hybrid TiO_2/NiO nanorods produced by the sol-gel technique showed high photocatalytic activity for the degradation of methylene blue (Baygi et al., 2020). Additionally, ZnO/NiO porous hollow spheres, which were produced by the calcination of Ni-Zn bimetallic organic frameworks, had noticeably more photocatalytic activity for the reduction of CO_2 as compared to pure ZnO or NiO (Lei et al., 2018). In addition, there are several benefits of depositing NiO onto g-C_3N_4. Firstly, NiO functions as a co-catalyst, facilitating effective charge transfer and electron-hole separation between the semiconductor and the chemical system. Furthermore, a large interfacial area is generated by the development of a NiO/g-C_3N_4 heterostructure, which enhances charge separation and facilitates the production of electron-hole pairs at the interface. Furthermore, effective photogenerated electron transfer from g-C_3N_4 to NiO is made possible by the heterojunction between NiO and g-C_3N_4, which reduces electron-hole

recombination even further and improves overall photocatalytic performance (Tao et al., 2024). ZnO combined with NiO may efficiently inhibit electron-hole recombination due to the synergistic interaction between the two semiconductors enabling pollutant degradation under both UV and visible light conditions (Sun et al., 2023).

Recently, researchers have also integrated graphitic carbon nitride (g-C_3N_4) with numerous semiconductors such as ZnO and NiO intending to substantially reduce recombination reactions resulting in enhanced sunlight absorption efficiency (Muhmood et al., 2024). g-C_3N_4 has drawn a lot of scientific interest considering its appropriate band gap (2.7 eV) successfully allowing visible light absorption (Panthi & Park, 2023). Furthermore, its inexpensive and non-toxic nature offers potential benefits in the photodegradation of organic pollutants and water splitting under visible light irradiation. Despite this, fast charge carrier recombination significantly reduces the photocatalytic efficiency of g-C_3N_4. To overcome the obstacle, several attempts have been rendered to improve the photocatalytic activity of g-C_3N_4 by combining it with other semiconductors and doping with metals or non-metals (Starukh & Praus, 2020). The development and fabrication of heterojunctions have emerged to be one of the most viable and efficient approaches for improving the photocatalytic efficiency of these mechanisms. Significantly higher photocatalytic activity has been observed in g-C_3N_4-based nanocomposites (such as g-C_3N_4/ZnO, g-C_3N_4/TiO_2, g-C_3N_4/CeO_2 and g-C_3N_4/CuO based nanocomposites) as compared to pure g-C_3N_4 (Mamba et al., 2024; Yuan et al., 2017).

This work provides an in-depth investigation of the facile synthesis, characterization, and utilization of g-C_3N_4/NiO/ZnO ternary nanocomposite-based photocatalyst for the degradation of methylene blue (MB) dye. Methylene blue (MB) was selected as the model organic pollutant due to its extensive industrial usage, environmental persistence, and ease of spectrophotometric detection, making it a representative and relevant dye for evaluating photocatalytic performance.

The ternary nanocomposite was successfully synthesized via a facile co-precipitation approach. A comprehensive characterization was performed employing numerous techniques such as XRD, RAMAN, SEM, UV-Vis, EIS, and PL spectroscopic techniques. The photocatalytic activity of g-C_3N_4/NiO/ZnO ternary nanocomposite-based photocatalyst was measured. The different factors including concentrations of the photocatalyst, and initial dye concentration were assessed to optimize the dye and photocatalyst concentrations for the potential use. Finally, the impact of scavengers and the reusability of the photocatalyst were investigated for stability. The utilization of g-C_3N_4/NiO/ZnO ternary nanocomposite-based photocatalysts in the degradation of MB is not yet covered in any currently available research. This investigation will further explore our comprehension of the photocatalytic activity, reusability, and catalytic characteristics of g-C_3N_4/NiO/ZnO ternary nanocomposite.

EXPERIMENTAL

Materials

Nickel nitrate hexahydrate ($Ni(NO_3)_2.6H_2O$), zinc nitrate hexahydrate ($Zn(NO_3)_2.6H_2O$), urea (CH_4N_2O), sodium hydroxide (NaOH), sodium carbonate (Na_2CO_3), ethanol (C_2H_5OH) and methylene blue (MB) dyes were purchased from Sigma Aldrich. The different solvents and reagents used in the study were of analytical grade and utilized devoid of any further purification.

Synthesis of g-C_3N_4/NiO/ZnO (CNZ) Nanocomposite

The facile co-precipitation approach was utilized to synthesize nanocomposite of zinc oxide, nickel oxide, and graphitic carbon nitride (g-C_3N_4/NiO/ZnO). The co-precipitation method was chosen due to its simplicity, cost-effectiveness, and ability to uniformly deposit multiple metal oxides onto the g-C_3N_4 matrix under mild conditions, facilitating the formation of a well-integrated ternary heterojunction. 2.90 g of nickel nitrate hexahydrate ($Ni(NO_3)_2.6H_2O$)

and 2.97 g of zinc nitrate hexahydrate ($Zn(NO_3)_2.6H_2O$) were mixed together in 50 ml distilled water. Afterward, g-C_3N_4 (100 mg) in 50 mL NaOH solution was added to the above dispersion under stirring. Dispersing g-C_3N_4 in NaOH produces deprotonated surface sites that electrostatically attract Zn^{2+}/Ni^{2+}. Subsequent base-induced co-precipitation forms $Zn(OH)_2$/$Ni(OH)_2$ nuclei *in situ* on/among the g-C_3N_4 nanosheets; calcination converts these hydroxides to ZnO and NiO, anchoring them across the g-C_3N_4 matrix and promoting a uniform distribution. The solution was vigorously stirred for 3 h to obtain a homogenous dispersion. The final product underwent an 8 h drying process after being thoroughly washed with ethanol and distilled water. The dry product was calcined for 3 h at 500 °C (@ ramp rate of 5 °C/min). Finally, the calcined powder was finely ground for subsequent analysis. The ternary nanocomposite was designated as CNZ for convenience. Figure 1 demonstrates the schematic design of g-C_3N_4/NiO/ZnO ternary nanocomposite-based photocatalyst. The NiO/ZnO, g-C_3N_4/ZnO, g-C_3N_4/NiO, ZnO, and NiO nanocomposites were synthesized using exactly the same procedure and were designated as NZ, CZ, CN, ZnO, and NiO, respectively. The g-C_3N_4 was prepared according to previous reports (Mo et al., 2015).

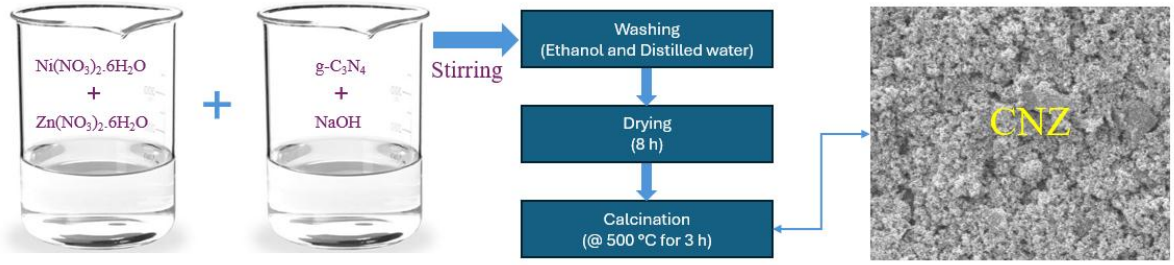

Figure 1. Schematic illustration of the synthesis scheme for CZN photocatalyst.

Measurement and Characterization

A Bruker D8 Advance diffractometer and BWS415-532S spectrophotometer were utilized for X-ray diffraction (XRD) and Raman analysis of the synthesized nanocomposites to gain insights into the structural mechanism. The morphology of g-C_3N_4/NiO/ZnO ternary nanocomposite and pristine ZnO, NiO, and g-C_3N_4 samples was studied using a Tescan VEGA 3 scanning electron microscope (SEM). A JENWAY spectrophotometer was used to record the UV-Vis absorption spectra in order to analyze the optical behavior. Bio-Logic VSP-1086 electrochemical workstation was utilized for the electrochemical impedance spectroscopic (EIS) analysis of the ternary nanocomposite. The charge transfer mechanism was examined using a photoluminescence spectrofluorometer.

The photocatalytic behavior of the CZN ternary nanocomposite was measured by monitoring the degradation of the dye (MB) in aqueous solution. Initially, the CZN ternary nanocomposite-based photocatalyst (0.05 g) was dispersed in an aqueous solution of MB (50 mL containing 10 mg/L). Prior to initiating the photoreaction, the mixture was thoroughly stirred for 90 minutes to establish an adsorption-desorption equilibrium, between the catalyst and the dye. To irradiate the solution, an 80 W xenon lamp was utilized to simulate sunlight. In order to avoid thermal catalytic effects and to keep the experiment at ambient temperature, cooling fans were employed. A spectrometer was used to determine the concentration of MB in a 10 mL sample collected at predetermined intervals. The concentration of the photocatalyst and the dye was also optimized and their influence on photocatalytic activity was examined. The reusability of CZN ternary nanocomposite-based photocatalyst was studied in comparison to commercially available ZnO nanoparticles solution up to 5 cycles. Electron capture tests were conducted using the same conditions in order to identify and scavenge the free radicals responsible for the degradation of MB.

Ethanol, silver nitrate, and isopropyl alcohol (0.05 mM) were added as scavengers for holes (h^+), electrons (e^-), and hydroxyl radicals (•OH), respectively.

RESULTS AND DISCUSSION

Figure 2a demonstrates the XRD pattern of different samples including g-C_3N_4, ZnO, NiO, CZ, and CNZ photocatalyst. The g-C_3N_4 sample exhibits a single diffraction peak at 27.60° well matching to (002) crystal face resulting from graphite structure (JCPDS No. 87-1526) affirming the existence of nanolayers of g-C_3N_4. Similarly, the XRD pattern of ZnO exhibited 2θ peaks at 31.81°, 34.62°, 36.27°, 47.70°, 56.68°, 63.11°, 66.44°, and 68.18° well correspond to (100), (002), (101), (102), (110), (103), (112), and (201) crystal planes of hexagonal wurtzite ZnO (JCPDS No. 36-1451), respectively, confirming the formation of ZnO nanoparticles (Fang et al., 2014). The XRD pattern of NiO exhibited three diffraction peaks at 2θ, 37.26°, 43.31°, and 62.73° matches with (111), (200) and (200) crystal planes of NiO (JCPDS No. 04-0835) (Narang et al., 2024). The XRD pattern of CZ was noted to be similar to that of ZnO with no peak observed for g-C_3N_4 might be due to the higher concentration of ZnO. However, no extra peak was observed due to the integration of g-C_3N_4 in ZnO corroborating the crystallinity of the nanocomposite. A slight change in peak position with a minor blue shift was observed for the target CNZ ternary nanocomposite. A new peak at 11.19° was observed in the CNZ sample corresponding to interlayer stacking of g-C_3N_4 nanosheets. Overall, the XRD pattern of CNZ ternary nanocomposite exhibited the successful incorporation of metal oxide semiconductors (ZnO and NiO) into g-C_3N_4.

Figure 2b displays the Raman spectra including g-C_3N_4, ZnO, NiO, and CNZ photocatalyst. Typically, graphitic carbon nitride has two noticeable bands that are slightly displaced. The existence of sp^3-hybridized carbon is suggested by the D band (1343 cm^{-1}), which can be explained by the material defects in structure and disordered regions. On the other hand, sp^2-hybridized carbon is linked to the G band (1596 cm^{-1}), which is in good agreement with previous reports (Machín et al., 2022). The Raman spectrum ZnO nanoparticles (NPs) demonstrated different peaks at 432 cm^{-1}, 577 cm^{-1}, 1041 cm^{-1}, and 1146 cm^{-1} corresponding to E_{2H}, E_1(LO), E_1(TO)+E_1(LO), 2P vibration modes of ZnO NPs (Sharma et al., 2012). The wurtzite structure of ZnO NPs is confirmed by a strong E_{2H} peak as corroborated by XRD measurements. NiO Raman spectrum exhibits characteristics peak of vibrational modes 1P TO mode (544 cm^{-1}), 1P LO (656 cm^{-1}), 2P LO+TO (1040 cm^{-1}), 2P LO (1261 cm^{-1}), and 2M (1731 cm^{-1}) (Gebretinsae et al., 2021). The Raman spectrum of CNZ ternary nanocomposite demonstrated slight displacement in peak positions attributed to the formation of an integrated structure produced by the incorporation of two metal oxide semiconductors (ZnO and NiO) into g-C_3N_4. However, the incorporation did not cause any noticeable change in the structure of ternary nanocomposite.

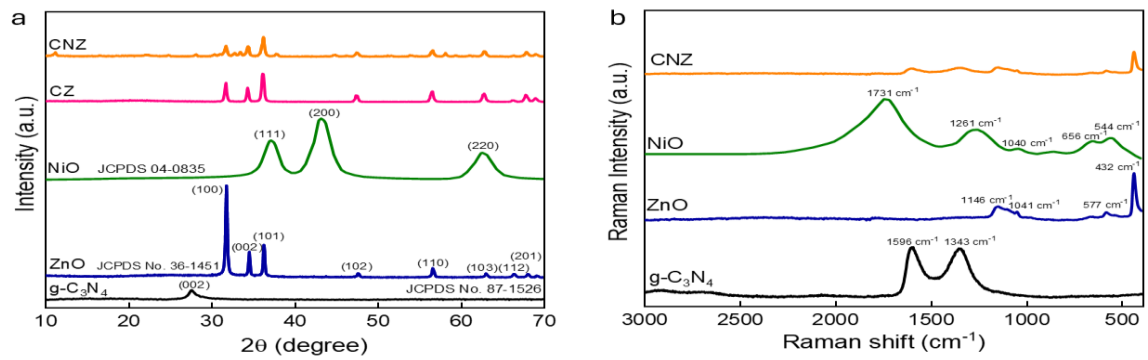

Figure 2. (a) XRD patterns of g-C_3N_4, ZnO, NiO, CZ, and CNZ photocatalyst, (b) Raman spectra of the g-C_3N_4, ZnO, NiO, and CNZ photocatalyst

The absence of extraneous peaks together with the 11.19° g-C_3N_4 stacking peak and slight peak shifts in CNZ indicate intimate interfacial integration rather than physical mixtures. The surface morphology of the pre-synthesized samples was examined by SEM. Figure 3

displays the SEM images of pure g-C_3N_4, ZnO, and NiO along CNZ ternary nanocomposite. The pure g-C_3N_4 (Figure 3a) resembles a stacked plate structure. This finding suggests that there is interconnectivity between the g-C_3N_4 sheets. ZnO exhibits morphology like spherical nanoparticles (Figure 3b) with a diameter ~ 50 nm and NiO also reveals nanoparticle morphology (Figure 3c) but due to agglomeration the exact size of NPs is crucial to estimate. The surface morphology of g-C_3N_4/NiO/ZnO ternary nanocomposite-based photocatalyst shows a random morphology with NiO and ZnO NPs anchored onto g-C_3N_4 nanosheets. The ternary nanocomposite generated a heterojunction structure that can effectively separate photogenerated charge carriers, increasing charge transfer efficiency and performance all around. The aggregation in Figure 3d also affirms the high surface area of the ternary nanocomposite, a prerequisite for effective degradations of pollutants. Although the particle size of ZnO (~50 nm) was visually estimated using SEM and the CNZ nanocomposite exhibited heterogeneous dispersion of particles, quantitative particle size distribution and BET surface area measurements were not performed in this study. Future investigations will focus on these characterizations to further correlate nanostructure features with photocatalytic performance. SEM (Fig. 3d) shows ZnO/NiO nanoparticles uniformly anchored across g-C_3N_4 sheets, with no large, segregated domains, consistent with uniform distribution imparted by *in situ* co-precipitation.

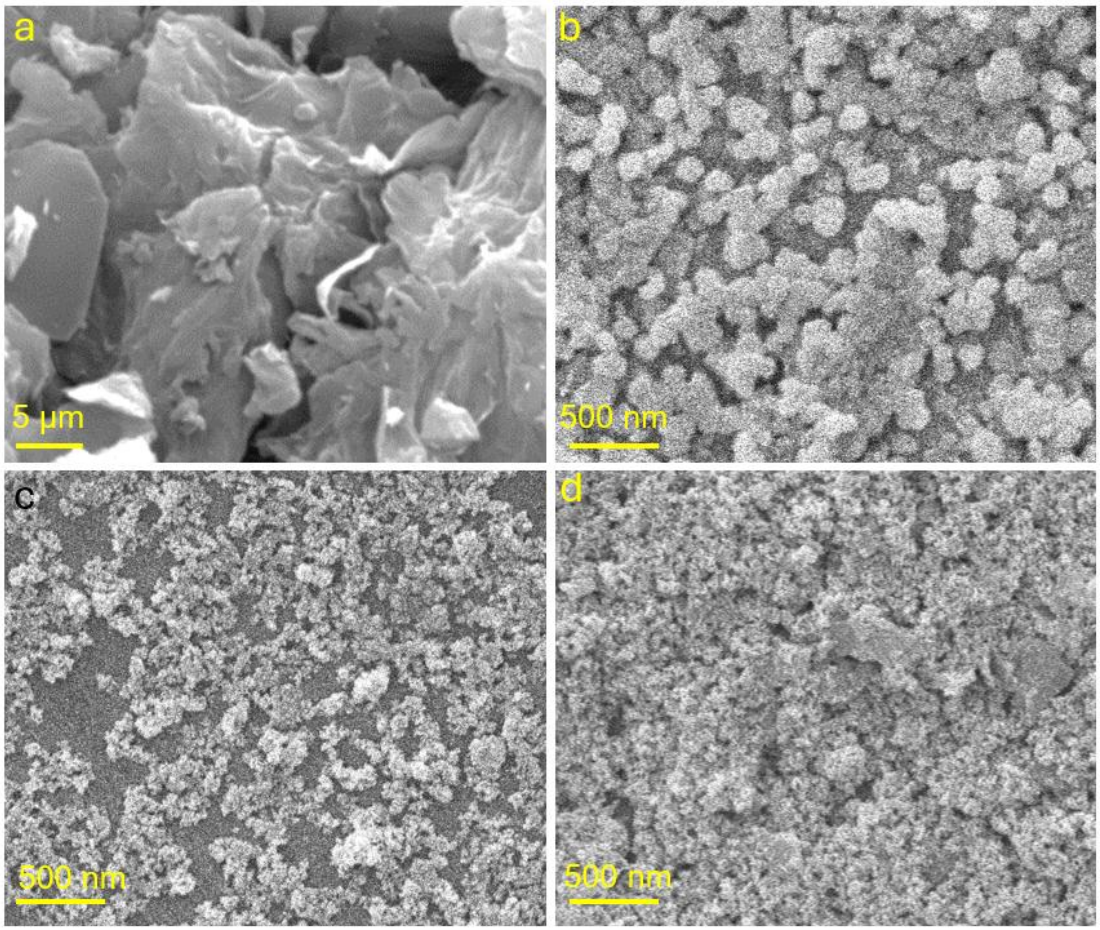

Figure 3. SEM images of (a) g-C_3N_4 nanosheets, (b) ZnO NPs, (c) NiO NPs, and (d) CNZ ternary nanocomposite.

UV-Vis absorption spectra were recorded at room temperature in order to evaluate the optical characteristics of pristine g-C_3N_4, NiO, ZnO, CZ, and CNZ photocatalysts. A narrow absorbance in the ultraviolet (UV) region was noticed for the majority of the synthesized samples (Figure 4a). However, CNZ revealed better light absorption and a noticeable

redshift in the absorption edge towards the visible range. The better light absorption and redshift in the absorption edge of CNZ ternary nanocomposite-based photocatalyst is consistent with previous studies on nanocomposites designed particularly for visible light absorption (Muhammad et al., 2024). The enhanced light absorption in the visible range and noticeable redshift indicate that absorption characteristics of CNZ ternary nanocomposite-based photocatalyst are successfully improved by integrating ZnO and NiO into g-C_3N_4 nanosheets. As a result, CNZ ternary nanocomposite is beneficial for photocatalytic processes as it can absorb more photons of visible light, encouraging the formation of electron-hole pairs and reactive species.

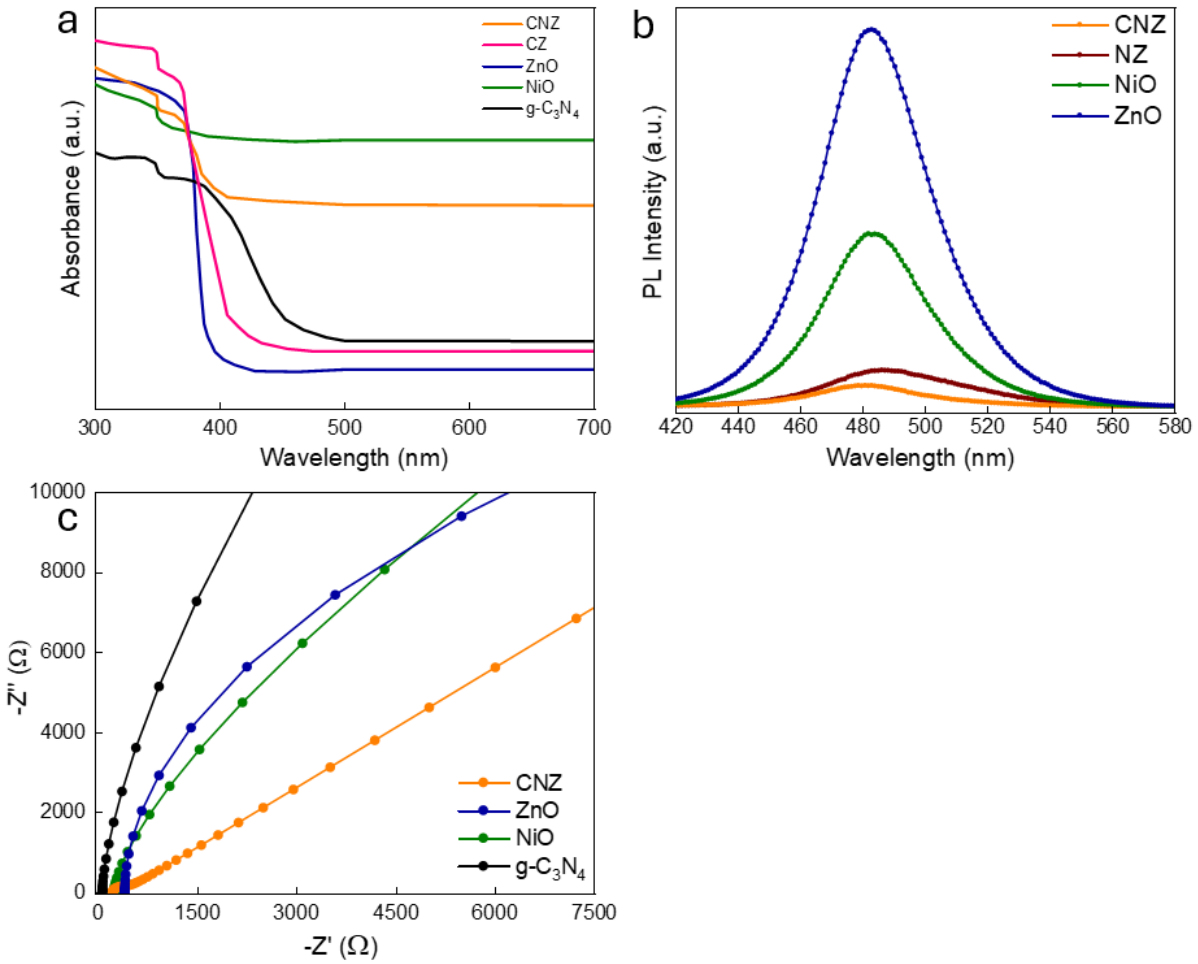

Figure 4. (a) UV-Vis absorbance spectra of g-C_3N_4, NiO, ZnO, CZ, and CNZ photocatalyst, (b) PL spectra of ZnO, NiO, NZ, and CNZ photocatalyst, and (c) EIS spectra of g-C_3N_4, NiO, ZnO, and CNZ photocatalyst.

The pronounced PL quenching and reduced Nyquist radius further evidence intimate heterointerfaces, which are enabled by the uniform dispersion of ZnO/NiO over g-C_3N_4. The PL spectra of ZnO, NiO, NZ, and CNZ are illustrated in Figure 4b. The emission spectra of ZnO NPs and NiO NPs exhibited highly intense but narrower peaks, suggesting an increased rate of charge carrier recombination. Nevertheless, a drop in PL intensity for NZ indicates that combining ZnO with NiO considerably lowers the recombination rate of electron-hole pairs. The CNZ ternary nanocomposite-based photocatalyst demonstrated a suppressed or lower peak intensity as compared to the NZ binary nanocomposite as well as NiO NPs and ZnO NPs. The results corroborate that the formation of heterostructures using g-C_3N_4, NiO, and ZnO may efficiently inhibit the recombination of electron-hole pairs generated during photocatalysis. Additionally, by inhibiting the photoinduced charge

carriers, the synergistic impact improves charge separation and reduces the rate at which photogenerated charge carriers recombine. Further evidence of the increased electron-hole separation in the CNZ ternary nanocomposite was provided by electrochemical impedance spectroscopy (EIS) analysis. The EIS spectra of g-C_3N_4, NiO, ZnO, and CNZ are shown in Figure 4c. The spectra demonstrate that CNZ has a lower arc radius in the Nyquist plot than the other samples, suggesting more effective transfer and separation of photogenerated charge carriers. The enhanced separation of photoinduced electron-hole pairs in CNZ is highlighted by this outcome. Although the redshift toward the visible region suggests better photon harvesting, enhanced photocatalytic efficiency requires synergistic improvements in charge separation and mobility. This is confirmed by PL quenching (Fig. 4b) and EIS spectra (Fig. 4c), which together affirm that CNZ possesses superior photoinduced charge dynamics and reduced recombination.

Due to its numerous potential applications in the field of solar energy conversion, photocatalysis has become a highly promising technology that might alleviate global energy constraints and environmental pollutants. Only 4% of ultraviolet (UV) radiation can be recognized in solar light, an endless natural energy source; visible light makes up a far bigger share (46%). Thus, boosting the photocatalytic efficiency of semiconductors in visible and ultraviolet light has emerged as a crucial field of investigation for optimizing solar energy utilization. To investigate the synergistic impact of the CNZ ternary nanocomposite-based photocatalyst, the photocatalytic activities of different photocatalysts were examined for the degradation of MB solution, a model organic pollutant, under visible light irradiation. All photocatalytic degradation experiments were performed in triplicate, and the reported degradation efficiencies represent the average values, with standard deviations consistently within ±2-3%, confirming the reproducibility of the results.

The photodegradation curves of MB to time using several samples of the photocatalysts under UV light irradiation are displayed in Figure 5a. With a photodegradation efficiency (PE) of 92% after 60 minutes of exposure, CNZ demonstrated the best performance among all the evaluated samples. In the same testing conditions, it outperformed other photocatalysts such as NZ (79% PE), CZ (82% PE), CN (60% PE), ZnO (77% PE), NiO (63% PE), and g-C3N4 (38% PE).

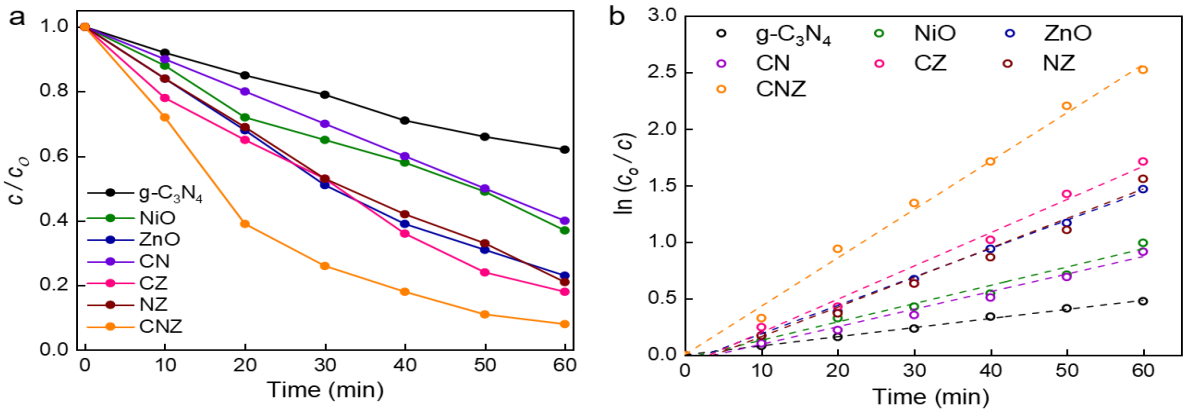

Figure 5. (a) Photocatalytic activity of MB using g-C_3N_4, Nio, ZnO, CN, CZ, NZ, CNZ photocatalysts, (b) kinetic analysis of the same.

To confirm the synergistic effect of the ternary system, control experiments using pure ZnO, NiO, and g-C_3N_4, along with binary composites (CZ, CN, NZ), were conducted under identical conditions. The CNZ ternary nanocomposite exhibited significantly higher degradation efficiency and kinetic rate constants compared to all controls, validating the cooperative interaction among the three components. The ternary nanocomposite CNZ exhibited the highest PE, followed by the CZ and NZ photocatalysts. These results suggest that the photocatalytic activity for pollutant degradation under irradiation is significantly

enhanced by the formation of CNZ ternary nanocomposite. In order to provide a quantifiable comparison of photocatalytic performance, a pseudo-first-order kinetic reaction model ($\ln(c/c_o)=kt$) was employed to analyze the collected data (Putri et al., 2019). The MB concentration at a given irradiation time is denoted by c in this equation, while the rate constant is denoted by k and the irradiation period is indicated by t. With a correlation coefficient (R^2) larger than 0.9, Figure 5b shows a strong linear connection, suggesting that the photocatalytic reaction follows first-order kinetics. Table 1 displays the k and R^2 values for each photocatalyst that was utilized in the photodegradation of MB. The rate constant *k* for MB degradation using CNZ ternary nanocomposite-based photocatalyst is estimated to be around 0.0427 min^{-1} quicker than the rate constants for CZ (0.0293 min^{-1}), CN (0.0155 min^{-1}), NZ (0.0261 min^{-1}), ZnO (0.0251 min^{-1}), NiO (0.0161 min^{-1}), and g-C_3N_4 (0.0080 min^{-1}). These findings imply that the CNZ photocatalyst discloses a much better MB degrading efficiency as compared to all other samples. Therefore, it can be presumed that CNZ can be utilized as an optimized photocatalyst for enhanced photocatalytic activity.

Table 1 k and R^2 values using different photocatalysts.

Photocatalysts	k (min^{-1})	R^2
CNZ	0.0427	0.9955
CZ	0.0293	0.9844
CN	0.0155	0.9841
NZ	0.0261	0.9807
ZnO	0.0251	0.9959
NiO	0.0161	0.9811
g-C_3N_4	0.0080	0.9973

We also measured the effect of CZN photocatalyst concentration and initial dye (MB) concentration by varying their masses to gain further insights into the optimization of the photocatalyst quantity and dye concentration. CZN photocatalyst concentration varied from 0.25 g/L to 1 g/L. The PE dramatically increased up to 0.75 g/L but then declined, as seen in Figure 6a. It has been established that increasing the photocatalyst concentration can result in the generation of further charge carriers and active species, both of which are essential for the degradation of MB. Agglomeration in the dye solution, on the other hand, can also result from using excessive photocatalyst which can reduce the quantity of light entering the solution and consequently decrease photodegradation efficiency. The optimal photocatalyst concentration was thus determined to be 0.75 g/L of CZN, which would enable effective light absorption and prevent the demand for additional catalysts. The effects of initial dye concentration were also evaluated across a range of 5 to 20 mg/L on the photodegradation of MB using 0.75 g/L of CZN. As shown in Figure 6b, the highest photocatalytic performance was noted for 15 mg/L MB concentrations.

There was a noticeable drop in the PE above this concentration. A higher concentration of MB can reduce the photoactivation of the catalyst for photodegradation since it can obstruct light from entering the reaction system. In addition, the PE decreases with increasing dye concentrations due to excess MB molecules which may block active sites and reduce their availability for photodegradation. In order to investigate the function of the energetic species in the photodegradation process of the CNZ ternary nanocomposite-based photocatalyst, trapping experiments were conducted and displayed in Figure 6c. It was probed out how different reactive species, such as hydroxyl radicals (•OH), holes (h^+), and superoxide radicals ($\bullet O_2^-$), contributed to photocatalytic degradation. To specifically quench these species, three types of trapping agents were used: $AgNO_3$ was used to trap O_2^- radicals, C_3H_8O for hydroxyl radicals, and C_2H_5OH was used to capture h^+. The results reveal that adding 0.05 mM $AgNO_3$ (electron scavenger) resulted in a slight decrease in the photocatalytic degradation of methylene blue (MB) over the CNZ ternary nanocomposite.

This indicates that the main active species involved in the degradation process are not photogenerated electrons. By contrast, the addition of C_3H_8O and C_2H_5OH (hydroxyl radicals and hole capture) greatly inhibited the photocatalytic activity. These results confirm that the primary oxidative species responsible for the photocatalytic degradation of MB are photogenerated holes and •OH radicals. Reusability is another crucial component in evaluating the practical performance of photocatalysts (Ahmadpour et al., 2024). The synthesized CZN photocatalyst exhibited remarkable stability as shown by Figure 6d by retaining 86% degradation efficiency for MB despite five cycles of reuse. The results confirm that CZN demonstrates long-term durability in photocatalytic applications. On the contrary, the degrading efficiency of MB using commercial ZnO decreased significantly with each cycle, reaching just over 62% after five cycles. The subsequent decrease in photocatalytic activity originates due to small particle size and high dispersion of ZnO, making it difficult to completely remove from the reaction system resulting in an enormous loss of ZnO powder.

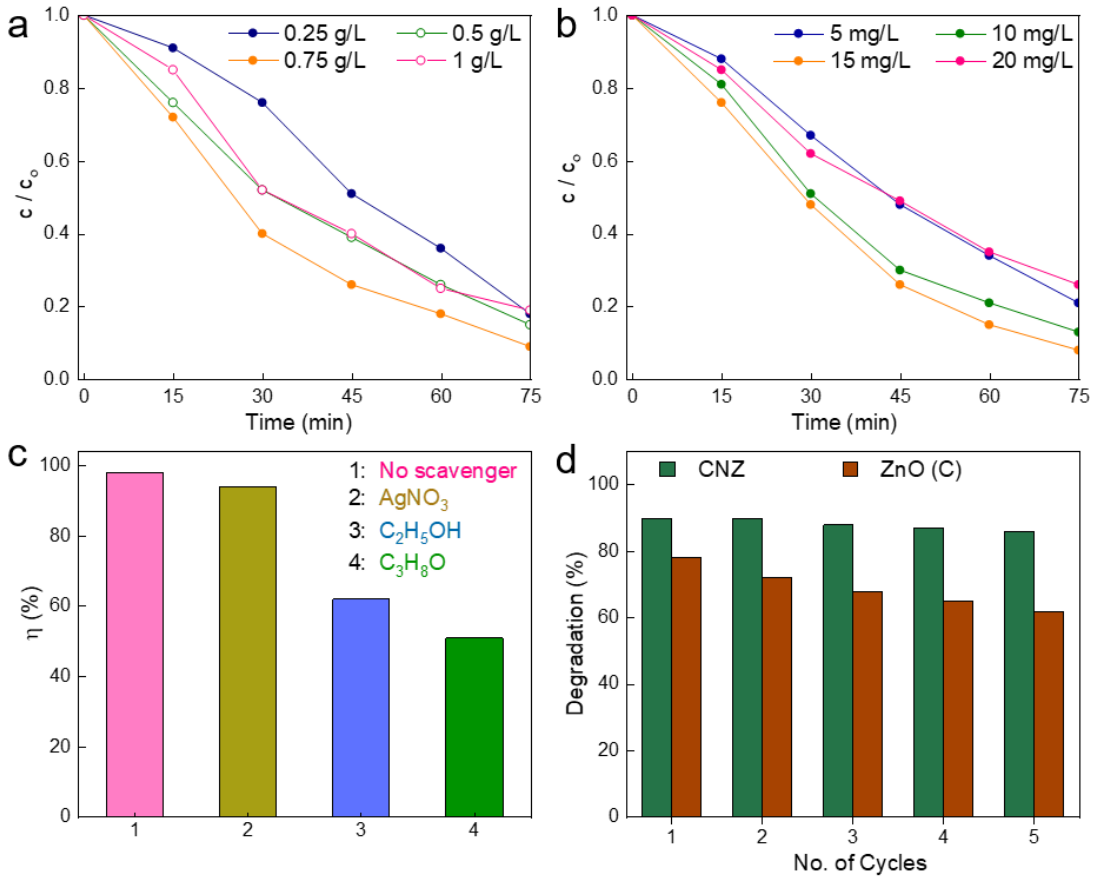

Figure 6. (a) Effect of photocatalyst concentration over MB degradation, (b) Effect of MB concentration over degradation, (c) Effect of scavengers on the degradation of MB, and (d) Reusability measurements.

In contrast, the better surface morphology and improved absorption of CZN ternary nanocomposite-based photocatalyst make solid-liquid separation simpler. These results highlight the stability and reliability of the CZN ternary nanocomposite-based photocatalyst for MB degradation in the presence of sunlight. The superior performance of the CNZ ternary nanocomposite can be ascribed to the synergistic effect of improved charge carrier separation, broader visible light absorption, and efficient heterojunction formation between g-C_3N_4, NiO, and ZnO, which collectively enhance photocatalytic activity.

Conclusions

The facile co-precipitation approach was employed to effectively synthesize a CNZ ternary nanocomposite-based photocatalyst, yielding substantial aggregates of g-C_3N_4, NiO, and ZnO. XRD and Raman studies confirmed the crystalline structure of ternary nanocomposite with high purity. Particularly, the nanocomposites show an extended absorption edge into the visible light spectrum, suggesting the potential of ternary nanocomposites, particularly for photocatalytic applications. CZN showed a significantly higher photoactivity than all other samples, achieving a degradation rate of 92% for MB. Further photocatalytic analysis revealed that a variety of parameters, such as initial MB concentration and photocatalyst quantity, influence the performance of CNZ. The ternary nanocomposites were also assessed by stability measurements over five successive reaction cycles confirming superior reusability in photocatalytic applications. The synergistic impact of the unique structure is mainly responsible for the improved photocatalytic performance. Furthermore, the degradation process is further enhanced by the increased number of active adsorption sites provided by the CNZ photocatalyst. We contemplate that combining distinct features of g-C_3N_4, NiO, and ZnO may realize possible applications in the fields of energy conversion and environmental purification, and open new avenues to develop more effective photocatalysts. Despite the promising photocatalytic performance of the CNZ nanocomposite, potential challenges such as synthesis scalability, catalyst recovery, and performance under real wastewater conditions must be addressed before practical application. Further studies involving real effluents, long-term durability, and catalyst immobilization strategies are warranted. Future work will involve testing the CNZ ternary nanocomposite on real wastewater samples to assess its photocatalytic performance under complex environmental conditions and evaluate its practical feasibility for industrial-scale water treatment.

Acknowledgment of Funding

This research did not receive any specific grant from funding agencies in the public, commercial, or not-for-profit sectors.

Declaration of No Conflicts of Interest

The authors declare that they have no known competing financial interests or personal relationships that could have appeared to influence the work reported in this manuscript.

Contributions of the Authors

All authors contributed significantly to the conception, design, synthesis, characterization, and analysis of the g-C3N4/NiO/ZnO-based ternary nanocomposite. Nimra Zafar, Affaf Sajjad, Rida Fatima, Taimoor Abbas, Muhammad Ajmal Khan, Muhammad Meesum Bilal, Uzma Bilal, Hafiz Muhammad Noman, and Abu Summama Sadavi Bilal collectively conducted the experimental work, data interpretation, and manuscript preparation. Abu Summama Sadavi Bilal served as the corresponding author and coordinated the research activities.

References

Ahmadpour, N., Nowrouzi, M., Madadi Avargani, V., Sayadi, M. H., & Zendehboudi, S. (2024). Design and optimization of TiO_2-based photocatalysts for efficient removal of pharmaceutical pollutants in water: Recent developments and challenges. *Journal of Water Process Engineering*, *57*, 104597. https://doi.org/10.1016/j.jwpe.2023.104597

Algarni, S., Tirth, V., Alqahtani, T., Alshehery, S., & Kshirsagar, P. (2023). Contribution of renewable energy sources to the environmental impacts and economic benefits for sustainable development.

Sustainable Energy Technologies and Assessments, *56*, 103098. https://doi.org/10.1016/j.seta.2023.103098

Alsukaibi, A. K. D. (2022). Various Approaches for the Detoxification of Toxic Dyes in Wastewater. *Processes*, *10*(10), 1968. https://www.mdpi.com/2227-9717/10/10/1968

Baygi, N. J., Saghir, A. V., Beidokhti, S. M., & Khaki, J. V. (2020). Modified auto-combustion synthesis of mixed-oxides TiO2/NiO nanoparticles: Physical properties and photocatalytic performance. *Ceramics International*, *46*(10, Part A), 15417-15437. https://doi.org/10.1016/j.ceramint.2020.03.087

Beura, R., Pachaiappan, R., & Thangadurai, P. (2018). A detailed study on Sn4+ doped ZnO for enhanced photocatalytic degradation. *Applied Surface Science*, *433*, 887-898. https://doi.org/10.1016/j.apsusc.2017.10.127

Bhapkar, A. R., & Bhame, S. (2024). A review on ZnO and its modifications for photocatalytic degradation of prominent textile effluents: Synthesis, mechanisms, and future directions. *Journal of Environmental Chemical Engineering*, *12*(3), 112553. https://doi.org/10.1016/j.jece.2024.112553

Chen, T., Liu, L., Hu, C., & Huang, H. (2021). Recent advances on Bi2WO6-based photocatalysts for environmental and energy applications. *Chinese Journal of Catalysis*, *42*(9), 1413-1438. https://doi.org/10.1016/S1872-2067(20)63769-X

Fang, L., Zhang, B., Li, W., Li, X., Xin, T., & Zhang, Q. (2014). Controllable synthesis of ZnO hierarchical architectures and their photocatalytic property. *Superlattices and Microstructures*, *75*, 324-333. https://doi.org/10.1016/j.spmi.2014.03.001

Flores-Diaz, N., De Rossi, F., Das, A., Deepa, M., Brunetti, F., & Freitag, M. (2023). Progress of Photocapacitors. *Chemical Reviews*, *123*(15), 9327-9355. https://doi.org/10.1021/acs.chemrev.2c00773

Gebretinsae, H. G., Tsegay, M. G., & Nuru, Z. Y. (2021). Biosynthesis of nickel oxide (NiO) nanoparticles from cactus plant extract. *Materials Today: Proceedings*, *36*, 566-570. https://doi.org/10.1016/j.matpr.2020.05.331

Han, Z., Liao, L., Wu, Y., Pan, H., Shen, S., & Chen, J. (2012). Synthesis and photocatalytic application of oriented hierarchical ZnO flower-rod architectures. *Journal of Hazardous Materials*, *217-218*, 100-106. https://doi.org/10.1016/j.jhazmat.2012.02.074

Kahouli, M., Barhoumi, A., Bouzid, A., Al-Hajry, A., & Guermazi, S. (2015). Structural and optical properties of ZnO nanoparticles prepared by direct precipitation method. *Superlattices and Microstructures*, *85*, 7-23. https://doi.org/10.1016/j.spmi.2015.05.007

Khader, E. H., Muslim, S. A., Saady, N. M. C., Ali, N. S., Salih, I. K., Mohammed, T. J., Albayati, T. M., & Zendehboudi, S. (2024). Recent advances in photocatalytic advanced oxidation processes for organic compound degradation: A review. *Desalination and Water Treatment*, *318*, 100384. https://doi.org/10.1016/j.dwt.2024.100384

Kumaresan, N., Sinthiya, M. M. A., Ramamurthi, K., Ramesh Babu, R., & Sethuraman, K. (2020). Visible light driven photocatalytic activity of ZnO/CuO nanocomposites coupled with rGO heterostructures synthesized by solid-state method for RhB dye degradation. *Arabian Journal of Chemistry*, *13*(2), 3910-3928. https://doi.org/10.1016/j.arabjc.2019.03.002

Lei, C., Pi, M., Cheng, B., Jiang, C., & Qin, J. (2018). Fabrication of hierarchical porous ZnO/NiO hollow microspheres for adsorptive removal of Congo red. *Applied Surface Science*, *435*, 1002-1010. https://doi.org/10.1016/j.apsusc.2017.11.201

Machín, A., Fontánez, K., Duconge, J., Cotto, M. C., Petrescu, F. I., Morant, C., & Márquez, F. (2022). Photocatalytic Degradation of Fluoroquinolone Antibiotics in Solution by Au@ZnO-rGO-gC3N4 Composites. *Catalysts*, *12*(2), 166. https://www.mdpi.com/2073-4344/12/2/166

Mamba, F. B., Mbuli, B. S., & Ramontja, J. (2024). Synergistic effect of ZnO/Ag2O@g-C3N4 based nanocomposites embedded in carrageenan matrix for dye degradation in water. *Heliyon*, *10*(11), e31109. https://doi.org/10.1016/j.heliyon.2024.e31109

Mo, Z., She, X., Li, Y., Liu, L., Huang, L., Chen, Z., Zhang, Q., Xu, H., & Li, H. (2015). Synthesis of g-C3N4 at different temperatures for superior visible/UV photocatalytic performance and photoelectrochemical sensing of MB solution [10.1039/C5RA19586A]. *RSC Advances*, *5*(123), 101552-101562. https://doi.org/10.1039/C5RA19586A

Muhammad, W., Khan, A., Hussain, S., Khan, H., Abumousa, R. A., Bououdina, M., Khan, I., Iqbal, S., & Humayun, M. (2024). Enhanced light absorption and charge carrier's separation in g-C3N4-based double Z-scheme heterostructure photocatalyst for efficient degradation of navy-blue dye.

Green Chemistry Letters and Reviews, *17*(1), 2381591. https://doi.org/10.1080/17518253.2024.2381591

Muhmood, T., Ahmad, I., Haider, Z., Haider, S. K., Shahzadi, N., Aftab, A., Ahmed, S., & Ahmad, F. (2024). Graphene-like graphitic carbon nitride (g-C3N4) as a semiconductor photocatalyst: Properties, classification, and defects engineering approaches. *Materials Today Sustainability*, *25*, 100633. https://doi.org/10.1016/j.mtsust.2023.100633

Narang, A. D., Gupta, S. P., Sanap, P. P., Kahandal, S. S., Tupke, R. S., Kim, H., Wang, Q., Vedpathak, A. S., Sartale, S. D., Gade, V. K., Shelke, P. B., Pawar, A. C., Kim, J. M., & Bulakhe, R. N. (2024). Development of nickel oxide thin film by chemical route for supercapacitor application. *Journal of Materials Science: Materials in Electronics*, *35*(19), 1335. https://doi.org/10.1007/s10854-024-12934-5

Natu, G., Hasin, P., Huang, Z., Ji, Z., He, M., & Wu, Y. (2012). Valence Band-Edge Engineering of Nickel Oxide Nanoparticles via Cobalt Doping for Application in p-Type Dye-Sensitized Solar Cells. *ACS Applied Materials & Interfaces*, *4*(11), 5922-5929. https://doi.org/10.1021/am301565j

Nishu, & Kumar, S. (2023). Smart and innovative nanotechnology applications for water purification. *Hybrid Advances*, *3*, 100044. https://doi.org/10.1016/j.hybadv.2023.100044

Onu, M. A., Ayeleru, O. O., Oboirien, B., & Olubambi, P. A. (2023). Challenges of wastewater generation and management in sub-Saharan Africa: A Review. *Environmental Challenges*, *11*, 100686. https://doi.org/10.1016/j.envc.2023.100686

Panthi, G., & Park, M. (2023). Graphitic Carbon Nitride/Zinc Oxide-Based Z-Scheme and S-Scheme Heterojunction Photocatalysts for the Photodegradation of Organic Pollutants. *International Journal of Molecular Sciences*, *24*(19), 15021. https://www.mdpi.com/1422-0067/24/19/15021

Putri, R. A., Safni, S., Jamarun, N., Septiani, U., Kim, M.-K., & Zoh, K.-d. (2019). Kinetics studies on photodegradation of methyl orange in the presence of C-N-codoped TiO2 catalyst. *Egyptian Journal of Chemistry*, *62*(Special Issue (Part 2) Innovation in Chemistry), 563-575. https://doi.org/10.21608/ejchem.2019.14543.1883

Qiu, R., Zhang, D., Mo, Y., Song, L., Brewer, E., Huang, X., & Xiong, Y. (2008). Photocatalytic activity of polymer-modified ZnO under visible light irradiation. *Journal of Hazardous Materials*, *156*(1), 80-85. https://doi.org/10.1016/j.jhazmat.2007.11.114

Raha, S., & Ahmaruzzaman, M. (2022). ZnO nanostructured materials and their potential applications: progress, challenges and perspectives [10.1039/D1NA00880C]. *Nanoscale Advances*, *4*(8), 1868-1925. https://doi.org/10.1039/D1NA00880C

Sahu, B., & Chopra, L. (2023). A review on removal of toxic colorants from the industrial effluent via advanced metal oxide semiconductor. *AIP Conference Proceedings*, *2535*(1). https://doi.org/10.1063/5.0138202

Samrot, A. V., Wilson, S., Sanjay Preeth, R. S., Prakash, P., Sathiyasree, M., Saigeetha, S., Shobana, N., Pachiyappan, S., & Rajesh, V. V. (2023). Sources of Antibiotic Contamination in Wastewater and Approaches to Their Removal—An Overview. *Sustainability*, *15*(16), 12639. https://www.mdpi.com/2071-1050/15/16/12639

Sharma, A., Singh, B. P., Dhar, S., Gondorf, A., & Spasova, M. (2012). Effect of surface groups on the luminescence property of ZnO nanoparticles synthesized by sol–gel route. *Surface Science*, *606*(3), L13-L17. https://doi.org/10.1016/j.susc.2011.09.006

Sikiru, S., Oladosu, T. L., Amosa, T. I., Olutoki, J. O., Ansari, M. N. M., Abioye, K. J., Rehman, Z. U., & Soleimani, H. (2024). Hydrogen-powered horizons: Transformative technologies in clean energy generation, distribution, and storage for sustainable innovation. *International Journal of Hydrogen Energy*, *56*, 1152-1182. https://doi.org/10.1016/j.ijhydene.2023.12.186

Starukh, H., & Praus, P. (2020). Doping of Graphitic Carbon Nitride with Non-Metal Elements and Its Applications in Photocatalysis. *Catalysts*, *10*(10), 1119. https://www.mdpi.com/2073-4344/10/10/1119

Sun, Y., Zhang, W., Li, Q., Liu, H., & Wang, X. (2023). Preparations and applications of zinc oxide based photocatalytic materials. *Advanced Sensor and Energy Materials*, *2*(3), 100069. https://doi.org/https://doi.org/10.1016/j.asems.2023.100069

Tao, F.-F., Dong, Y., & Yang, L. (2024). NiO/g-C3N4 p–n Heterojunctions Wrapped by rGO for the Enhanced CO_2 Photocatalytic Reduction. *ACS Sustainable Chemistry & Engineering*, *12*(17), 6709-6718. https://doi.org/10.1021/acssuschemeng.4c00579

Toma, E. E., Stoian, G., Cojocaru, B., Parvulescu, V. I., & Coman, S. M. (2022). ZnO/CQDs Nanocomposites for Visible Light Photodegradation of Organic Pollutants. *Catalysts*, *12*(9), 952. https://www.mdpi.com/2073-4344/12/9/952

Wang, L., Dong, Y., Zhang, J., Tao, F., & Xu, J. (2022). Construction of NiO/g-C3N4 p-n heterojunctions for enhanced photocatalytic CO_2 reduction. *Journal of Solid State Chemistry*, *308*, 122878. https://doi.org/10.1016/j.jssc.2022.122878

Xu, X., Wu, C., Guo, A., Qin, B., Sun, Y., Zhao, C., Zhang, F., & Cai, A. (2022). Visible-light photocatalysis of organic contaminants and disinfection using biomimetic-synthesized TiO_2-Ag-AgCl composite. *Applied Surface Science*, *588*, 152886. https://doi.org/10.1016/j.apsusc.2022.152886

Yang, R., Zhang, Y., Fan, Y., Wang, R., Zhu, R., Tang, Y., Yin, Z., & Zeng, Z. (2022). InVO4-based photocatalysts for energy and environmental applications. *Chemical Engineering Journal*, *428*, 131145. https://doi.org/https://doi.org/10.1016/j.cej.2021.131145

Yuan, Y., Huang, G.-F., Hu, W.-Y., Xiong, D.-N., Zhou, B.-X., Chang, S., & Huang, W.-Q. (2017). Construction of g-C3N4/CeO2/ZnO ternary photocatalysts with enhanced photocatalytic performance. *Journal of Physics and Chemistry of Solids*, *106*, 1-9. https://doi.org/10.1016/j.jpcs.2017.02.015

Zeinali Heris, S., Etemadi, M., Mousavi, S. B., Mohammadpourfard, M., & Ramavandi, B. (2023). Preparation and characterizations of TiO2/ZnO nanohybrid and its application in photocatalytic degradation of tetracycline in wastewater. *Journal of Photochemistry and Photobiology A: Chemistry*, *443*, 114893. https://doi.org/10.1016/j.jphotochem.2023.114893

Zhang, H., Liu, J., Xu, T., Ji, W., & Zong, X. (2023). Recent Advances on Small Band Gap Semiconductor Materials (≤2.1 eV) for Solar Water Splitting. *Catalysts*, *13*(4), 728. https://www.mdpi.com/2073-4344/13/4/728

Zhang, J., Wu, H., Shi, L., Wu, Z., Zhang, S., Wang, S., & Sun, H. (2024). Photocatalysis coupling with membrane technology for sustainable and continuous purification of wastewater. *Separation and Purification Technology*, *329*, 125225. https://doi.org/10.1016/j.seppur.2023.125225

Zhang, L., Jia, C., Bai, F., Wang, W., An, S., Zhao, K., Li, Z., Li, J., & Sun, H. (2024). A comprehensive review of the promising clean energy carrier: Hydrogen production, transportation, storage, and utilization (HPTSU) technologies. *Fuel*, *355*, 129455. https://doi.org/10.1016/j.fuel.2023.129455